TAO, Vol.1, No.4, PP.379-391, December 1990

Modified Eady Waves and Frontogenesis Part II: Nonlinear Integration

WEN-YIH SUN
Department of Earth and Atmospheric Sciences
Purdue University, W. Lafayette, IN 47907, U.S.A.

(Received 5 November 1990; revised 30 December 1990)

ABSTRACT

The stability analysis of the modified Eady waves (Eady, 1949) in a constant shear flow with parabolic temperature profiles has been discussed in Part I. Here, we apply the nonlinear model developed at Purdue University to study the evolution of those unstable waves obtained from Part I. The long waves (referred to as Mode I in Part I) develop into fronts with the maximum perturbations of pressure and temperature being either at the top or at the bottom of the domain. They are similar to conventional Eady waves discussed by Williams (1967) and Hoskin (1978), although the amplitudes of the simulated perturbations near the top are smaller than those near the bottom, due to a stronger stratification in the upper atmosphere in our parabolic temperature profiles. The short waves (referred to as Mode II in Part I), which need more time to develop into a front, are confined to the lower atmosphere. The modeling phase speed of the short waves is much slower than the conventional baroclinic waves, as predicted in Part I.

Both stability analyses and nonlinear integrations confirm that the surface wave/front can develop and reach finite amplitude within a few days, when the stratification in the lower atmosphere is weak. The results of this study may be related to the development of the medium scale disturbances observed over the Kuroshio Current and East China Sea during the winter.

1. INTRODUCTION

Instability of the modified Eady waves has been presented by Sun (1989). His results show that, in addition to the long waves (Mode I), the short waves (mode II) can also develop in the lower atmosphere, where the stable stratification is weaker than that in the upper atmosphere. From both stability analysis and energy conversions of those waves, Sun found that for the short waves, the

disturbances become more unstable under a more stable stratification aloft, which is quite different from the conventional Eady waves and other studies. Hence, Sun (1989) has introduced an effective Burger number in order to explain the growth rate of the baroclinic waves with parabolic temperature profiles.

The time evolution of the baroclinic disturbances of the classical Eady problem has been documented by Stone (1966), Williams and Plotkin (1968), and Williams (1968). Such results show that the perturbation fields grow exponentially in time, but that the "front" formed in the quasi-geostrophic system has large negative and positive relative vorticities, without a vertical tilt. Obviously, the quasi-geostrophic approximation has a rather indefinite view of the development of the baroclinic perturbations. When the magnitude of the relative vorticity increases, the nonlinear advection terms soon become important in comparison with the Coriolis parameter, which invalidates the quasi-geostrophic theory.

Later, the semi-geostrophic equations were used for some theoretical studies of the classical baroclinic problem in an adiabatic, inviscid flow (Hoskins, 1971; Hoskins and Bretherton, 1972; Blumen, 1979, 1980; Hoskins and Heckley, 1981). By using geostrophic balance in the cross-front direction but not the along-front direction, their results displayed a front that tilts with height toward the cold air, as is observed in Williams' results. The semi-geostrophic approximation is an important tool to study frontogenesis in an inviscid fluid with simple wind and temperature distributions. But it is not convenient to apply in a more realistic situation. Thus, we shall employ the fully nonlinear, hydrostatic primitive equations in our model instead of using the semi-geostrophic equations.

Here, a two-dimensional version of the Purdue mesoscale model (Sun and Hsu, 1984; Sun and Hsu, 1988) is applied to study the evolution of the baroclinic waves and frontogenesis. The eigen functions generated by the linearized equations (Kao,1978; Sun 1989) are used as the initial conditions. A numerical experiment of the Eady wave (Williams; 1967) is reproduced in order to test the accuracy and efficiency of our model. The surface front associated with Mode II is also generated by this model, which confirms that the short wave can develop into a front in the lower atmosphere under a weak stable stratification.

Recently, Orlanski (1986) applied a two-dimensional nonlinear model to study the evolution of the surface waves in an atmosphere with piecewise-linear temperature lapse rates. His results show that the short surface waves develop in a less-stably stratified lower atmosphere as we obtained. Orlanski also found that the mesoscale baroclinic waves can grow much faster with localized surface heating.

Here, we present only the results for idealized cases in a dry, inviscid, adiabatic atmosphere. Currently, we are using the three-dimensional model, which includes the effects of condensation, radiation, turbulent transports of heat,

moisture and momentum, as well as a detailed planetary boundary layer, to study the observed medium scale disturbances and surface frontogenesis.

2. FUNDAMENTAL EQUATIONS AND NUMERICAL MODEL

a. The sigma coordinates

A normalized pressure coordinate is employed in the Purdue mesoscale model. This vertical coordinate σ is defined as

$$\sigma = (p - p_t)/p^*, \tag{2.1}$$

with

$$p^* = p_s - p_t, \tag{2.2}$$

where the pressure p_t is a constant pressure at the top boundary of the domain, and p_s=1000 mb is the surface pressure.

Since the eigenfunctions of the modified Eady model are calculated in another coordinate system (x, y, z (pseudo height), t), some coordinate transformations are required before integration. The eigenfunctions can be converted from the z to the σ system, since both pseudo height and σ are functions of pressure. However, the variation of the horizontal components of dependent variables in σ coordinate are no longer as simple as in the z coordinate.

Since a two-dimensional model is employed in this study, the three-dimensional system of primitive equations has to be reduced to two dimensions (x,σ) by specifying the y variation of the horizontal components of all dependent variables. The conditions on u and v are

$$\frac{\partial u}{\partial y_z} = \frac{\partial v}{\partial y_z} = 0, \tag{2.3}$$

and the y variation of θ is

$$\frac{\partial \theta}{\partial y_z} = -\frac{f\theta_0 V}{gH}. \tag{2.4}$$

When the above conditions from the pseudo-height system are converted to the σ system, the latitudinal variations on u, v, θ and p^* become:

$$\frac{\partial u}{\partial y_\sigma} = \frac{\partial u}{\partial \sigma}\frac{f}{p^*}(-\sigma p_s U_{gs}), \tag{2.5}$$

$$\frac{\partial v}{\partial y_\sigma} = \frac{\partial v}{\partial \sigma}\frac{f}{p^*}(-\sigma p_s U_{gs}), \tag{2.6}$$

$$\frac{\partial \theta}{\partial y_\sigma} = \frac{\partial \theta}{\partial y_z} + \frac{\partial \theta}{\partial \sigma} \frac{f}{p^*}(-\sigma \rho_s U_{gs}), \tag{2.7}$$

and

$$\frac{\partial p^*}{\partial y_\sigma} = -\rho_s f u_{gs}, \tag{2.8}$$

where the subscript s refers to the surface $p = p_s$.

b. The model

In this investigation, the atmosphere is assumed to be dry, hydrostatic, inviscid and fully compressible. The fundamental equations are identical to those presented by Sun and Hsu (1984, 1988), except here the diffusion and moisture are completely ignored. The forward-backward scheme (Sun, 1980; 1984) is applied to handle the inertial gravity waves with a short time interval. The horizontal advection is integrated with a larger time interval limited by the CFL criterion of the advection equation (Sun and Hsu, 1988). A uniform space interval $\Delta x = 50$ km is utilized in the x direction for every experiment. There are 25 levels with a uniform $\Delta\sigma$ in the vertical direction for the numerical experiments of the classical Eady problem and the long waves of the modified Eady problem. There are 50 levels in the vertical direction for the short wave perturbations, because a high resolution is required for the short waves, which mainly occur in the lower portion of the domain.

3. NUMERICAL RESULTS AND DISCUSSIONS OF FRONTOGENESIS

As discussed in introduction, the two-dimensional version of the Purdue mesoscale model will be applied to investigate the development of the the baroclinic waves (i.e., eigen values) obtained from Part I. The fronts generated by Williams (1967) were used as references to verify our numerical model. Hence, the comparisons between Williams' results and ours will be discussed. The numerical simulations of the modified Eady waves will follow.

a. Simulations with constant lapse rates

The numerical integration of the Eady problem in a Boussinesq fluid was first presented by Williams (1967). He considered a constant shear flow that is antisymmetric at the mid-level. Therefore, the relative phase speed of his baroclinic perturbation becomes zero, which results in a stationary frontal zone after a finite period of time integration. To test our mesoscale model, we integrate from the same initial fields as did Williams (1967). The constants which define the initial state are

$S = 3\ m\ s^{-1}$, $H = 9\ km$,
$\theta_o = 300\ K$, $p_t = 297.709\ mb$,
$\partial\theta/\partial y = -10^{-5}\ K\ m^{-1}$, $p_s = 1000\ mb$,
$\partial\theta/\partial z = 3.9\ K\ km^{-1}$, $L = 2000/\pi\ km$,
and $\lambda = 4000\ km$.

Despite the smaller extremes of the v' and the θ' fields at our five days' integration (not shown here), the agreement between our numerical experiment and Williams' experiment is good. The magnitude of the vorticity in the cyclonic region is larger than in the anticyclonic region, although their initial values are the same. The characteristic of stronger along-front velocity gradient in the cyclonic region is preserved. It is noted that the region of the maximum vorticity, i.e., the maximum $\partial v/\partial x$, propagates from the initial location of $x \approx 500\ km$ to $x \approx -60\ km$ with a mean westerly wind of $1.3\ m\ s^{-1}$, although a stationary front is obtained in Williams' hydrostatic Boussinesq fluid, the wind at the steering level is negative in our compressible fluid and the front moves westward, as expected.

The geostrophic approximation is still valid across the front (Williams, 1967; Hoskins, 1978). However, the nonlinear terms distort the quasi-geostrophic solution near the front to produce a fairly realistic front. The amplitude of the u perturbation field now is of the order of $10\ m\ s^{-1}$ (not shown here), which suggests that the across-front velocity, as well as the horizontal divergence, can no longer be neglected and so causes distortion in baroclinic waves.

The strength of the front in our model is weaker than Williams' prediction. This is mainly due to the fourth order Shuman smoothing (Shuman, 1957) introduced in our model, and partly due to the different round-off errors inherent in different numerical integration schemes. However, the characteristics of the fronts remain the same.

The other cases with a constant temperature lapse rate and a constant wind shear in a westerly flow ($v = V \times z/H$, whit $V > 0$) have also been tested. The patterns are very similar to the previous case, except fronts move eastward, as observed in the mid-latitude. The results also reveal that long waves grow faster in the atmosphere with a weaker stratification. The westward tilt of v' is also larger in a weak stable stratification than in a strong stable stratification. However, the propagation speed of fronts is about the same.

b. Simulation with variable lapse rate and surface frontogenesis

Stability analysis in Part I shows that the general features of eigenfunctions of the long waves in Mode I are similar to the classical Eady wave. However, the growth rates, vertical structure, and phase speeds of perturbations of long waves differ from those of the short waves in Mode II. If fronts are generated

from both Modes with the same amplitude, after a finite period of time, the fronts associated with Mode II will be weaker and propagate more slowly. It is also expected that unstable waves and the corresponding front of Mode II will be confined in the low levels, and so lead to a surface front.

The growth rate of unstable waves in Mode II increases with the increase of stable stratification in the upper atmosphere. Since the vertical structure of eigenfunctions is similar among the waves in Mode II, case 2e is chosen as a representative example. The initial temperature profiles for case 2a to 2e are given by

$$\theta = az^2 + bz + \theta_0 + (\partial\theta/\partial y)y. \tag{3.1}$$

The constants are: $a = n \times del$, where $n = 1, 2, 3, 4, 5$ for cases 2a to 2e; $del = 0.05\ K\ km^{-2}$; $b = 2.0\ K\ km^{-1}$; $q_0 = 288\ K$, and $\partial q/\partial y = -10^{-2}\ K\ km^{-1}$, as discussed in Part I.

The numerical simulations are applied to both long and short waves. The wave number for long wave is $\alpha_1 = 0.5 \times \pi$ (i.e, wavelength $\lambda = 4000\ km$) while that for short wave is $\alpha_2 = 1.25 \times \pi$ (i.e., wavelength= 1600 km). The initial perturbation fields of v' and θ' for $\lambda = 4000\ km$ are shown in Figs. 7 and 8 of Part I, which are obtained from linear stability stability analysis. The initial v' and θ' are slightly larger in the lower region than those in the upper region. After five days integration, the general features are similar to the standard Eady model simulation. The system propagates eastward at a speed of 13 $m\ s^{-1}$, which is about the mean wind at 650 mb ($\approx$ 3.6 km above the ground). A large distortion is caused by deformation such that a cold frontal zone is created in the region of maximum cyclonic shear (Figs. 1-4). For the long waves, the strength of the front for case 2e is smaller than for the other cases, as predicted in Part I. Though the vorticity field is stronger at the surface than it is at the top boundary, fronts still show at both the top and bottom boundaries. As can be seen in the vertical velocity field (Fig. 5), a stronger upward motion ($w \approx 3.1\ cm\ s^{-1}$) exists on the warm side of the cold front, and a downward motion on the cold side. Both tilt westward with height with the cold frontal zone. We can see that a warm air parcel in the lower troposphere coming from the south moves toward north and ascends gradually ahead of the cold front, while the cold air coming from the north moves south and descends behind the front. The slope of the warm front, which is defined as the cold air mass is replaced by a warm air mass, is smaller than that of the cold front (Fig. 4). The intensity of the cold front is also much stronger as expected. A strong southerly wind ahead of the cold front, but a northerly wind behind indicates a strong cyclonic flow along the cold frontal zone.

The initial perturbations for case 2e with $\lambda = 1600\ km$ are shown in Figs. 11-12 of Part I. The initial v' field is confined to the lower region and has a steep westward tilt compared to the long wave. After six days' integration, a frontal

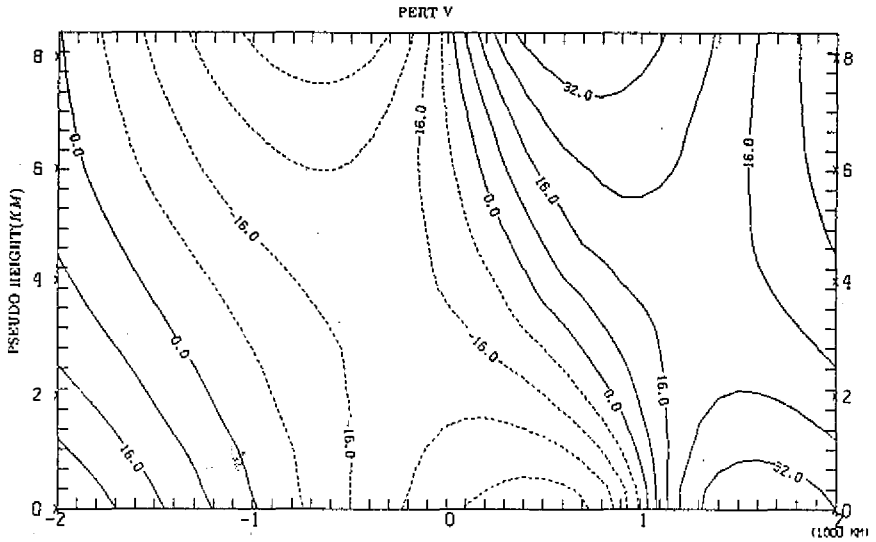

Fig. 1. The simulated perturbation field v' at $t = 5$ days for $\lambda = 4000\ km$ in case 2e of the modified Eady model.

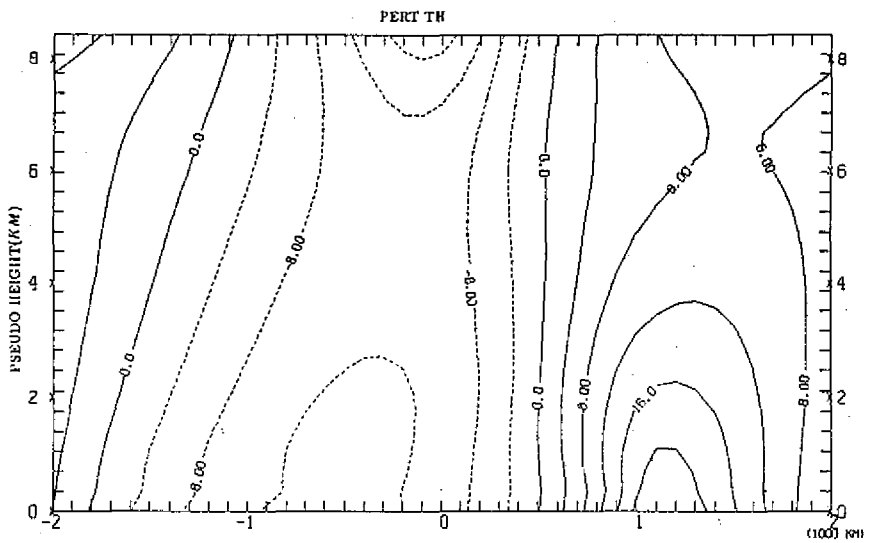

Fig. 2. Same as *Fig.* 1 except for the θ' field.

zone is completely embedded within the cyclonic region (Figs. 6-7). The system propagates with a velocity of 4.6 $m\ s^{-1}$, which is very close to the value of 4.8 $m\ s^{-1}$ predicted in linear stability analysis. The fact that the eigenvalue c_i is smaller for Mode II leads to a correspondingly weaker shear gradient, $\partial v/\partial x$, in this experiment. It is important to note that even though the velocity field is not strong in this case, deformation still distorts the perturbation fields in the

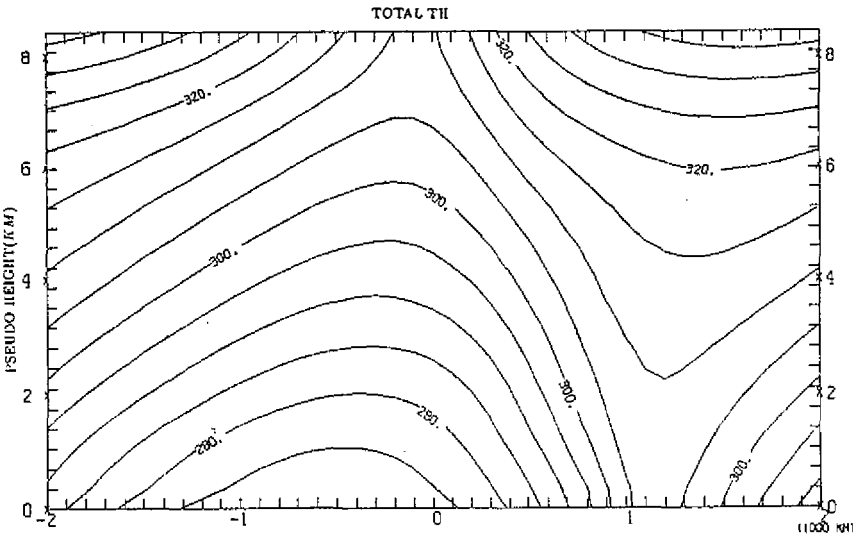

Fig. 3. Same as *Fig.* 1 except for the total θ field.

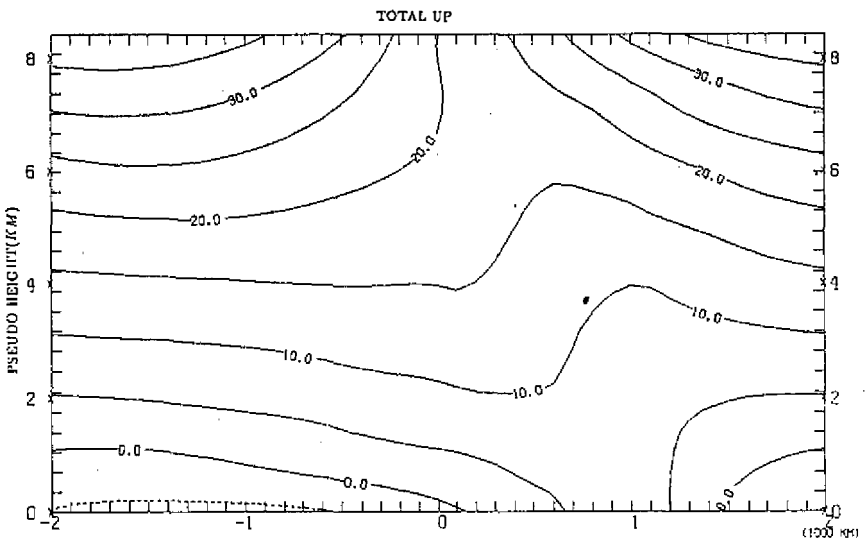

Fig. 4. Same as *Fig.* 1 except for the total u field.

same way: namely, the growth rates of the v' and θ' fields in the cyclonic region are larger than in the anticyclonic region. In this case, fronts are produced with the maximum along-front velocity value of only 20 $m\ s^{-1}$ and the maximum thermal perturbation of 7.7 K (Figs. 6-7). These values are smaller than that generated from the longwave perturbation.

The vertical velocity field (not shown here) indicates that the warm air

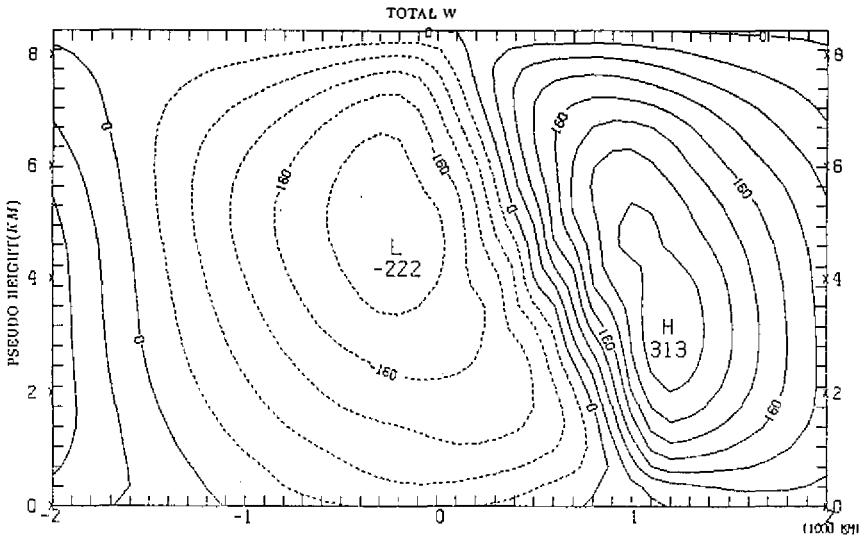

Fig. 5. Same as *Fig.* 1 except for the vertical velocity field $w = dz/dt$.

coming from the south is rising ahead of the frontal zone while the cold air coming from the north is sinking behind. The maximum upward reaches 2.7 $cm\ s^{-1}$ and is located at the level of 1.7 km above the ground. Hence, the fully-developed waves (or a weak front) remains in the lower layer, where the stable stratification is weak. Like a typical cold front in the mid-latitude, a southerly wind is accompanied with upward motion ahead of the front; the frontal passage is immediately followed by descending motion with northerly wind. The warm front is very diffused in the the Mode II region.

Generally speaking, cold frontal zones (large positive vorticity regions) are caused by the divergence effect and/or by deformation. As was the case for Mode II, the short waves can be initialized by sub-synoptic scale disturbances. It can also be produced from nonlinear interaction of synoptic scale disturbances, or by the effect of latent heat or other mechanisms. The simulated short waves are confined to low levels, as predicted in linear stability analysis. They are also comparable to the short waves discussed by Orlanski (1987). This study also suggests that frontogenesis may proceed in both small scale as well as in synoptic scale systems. As discussed in Part I, during the winter, the medium-scale disturbances (with wavelengths of about 1000-2000 km) in the West Pacific Ocean become active in a moist lower troposphere under conditions of a less stable thermal stratification, and are not associated with an upper tropospheric trough. They align in the west-east direction with less tilt of the phase angles in the vertical direction than that of the conventional baroclinic waves. Those disturbances may be associated with the unstable waves

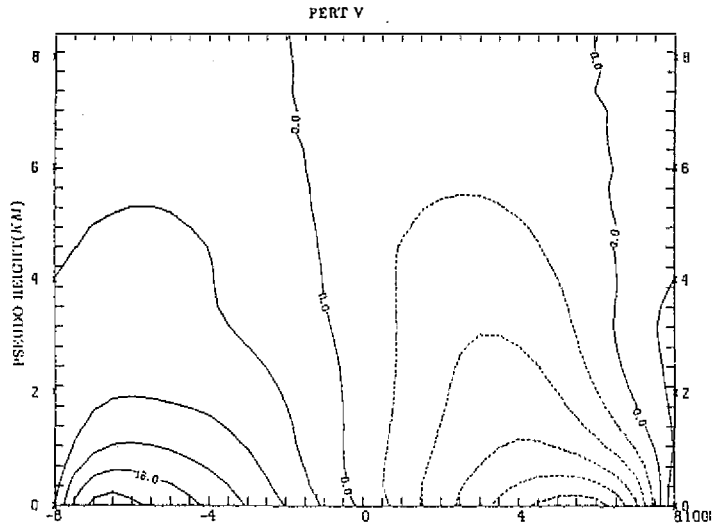

Fig. 6. The simulated v' at $t = 6$ days for λ =1600 km in case 2e.

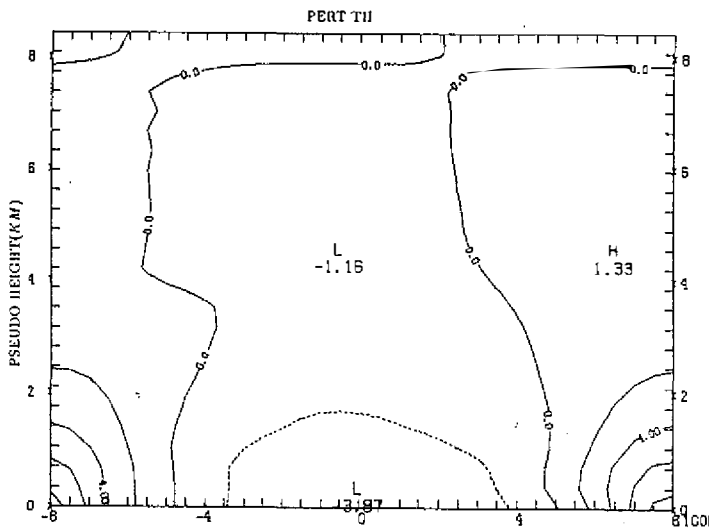

Fig. 7. Same as *Fig.* 6 except for the θ' field.

(or fronts) of Mode II discussed here. More study is required in order to understand the energy conversion and effect of the latent heat on the evolution of unstable waves and fronts simulated here. It is also believed that both real data simulation and sensitivity tests are required in order to further understand the medium-scale disturbances in the West Pacific Ocean and other places during the winter.

4. SUMMARY

It has been shown from the modified Eady model that the spectrum of baroclinic disturbances for a parabolic potential temperature profile consists of a short wave band and a long wave band. The unstable waves in the short wave band (Mode II) are confined to the lower troposphere and the long wave disturbances (Mode I) extend to the entire troposphere. The wave number of transition between these two bands decreases with increasing stratification.

Eady-type eigenfunctions have been found in the long wave region (Mode I). The growth rate of the Mode I perturbation decreases with increasing stratification; the perturbation is larger at the surface than it is at the top boundary, and the relative speed is slightly less than the mean velocity of the flow. On the other hand, the growth rate of the unstable wave in the short wave region (Mode II) increases with increasing stratification. The relative phase speed decreases more quickly with increasing wave number, and the perturbation is confined to the lower troposphere.

Here, the numerical results from a nonlinear model show that the fronts can develop from weak baroclinic waves within a few days. The cold frontal zones are more prominent from both the long wave and short wave simulations. The negative vorticity in the anticyclonic region is smaller than the positive vorticity value in the cyclonic region. The development of the front in Mode II is slower than Mode I, due to a small growth rate, as discussed in Part I. However, the short waves may develop rapidly when the latent heat and/or localized heating is included. The short waves/front obtained here may be associated with the medium-scale disturbances observed over the Kuroshio Current and surrounding area during the winter, where the stable stratification is weak in the moist lower atmosphere. Latent heat is important in the development of the medium-scale disturbances in the real atmosphere. In the next study, the effect of condensation and eddy diffusion will be incorporated. The real data simulations will also be carried out by using a complete three-dimensional model.

Acknowledgements. Contributions of Ms. R. L. Kao and Mr. A. Yildirim on this work are appreciated. Part of this work was supported by NSF under grant ATMS-8611729 and ATM-8907881.

REFERENCES

Blumen, W., 1979: Unstable nonlinear evolution of and Eady Wave in time dependent basic flows and frontogenesis. *J. Atmos. Sci.*, **36**, 3-11.

____, 1980: A comparison between the Hoskins-Bretherton model of frontoge-

nesis and the analysis of an intense surface frontal zone. *J. Atmos. Sci.*, **37**, 64-77.

Eady, E. T., 1949: Long waves and cyclone waves. *Tellus*, **1**, 33-52.

Hoskins, B. J., 1971: Atmospheric frontogenesis: some solutions. *Quart. J. Roy. Meteor. Soc.*, **97**, 139-153.

____, 1978: *Baroclinic Instability and Frontogensis in Rotating Fluids in Geophysics.*, P. H. Roberts, ed., Academic Press. 171-204.

____, and F. P. Bretherton, 1972: Atmospheric frontogenesis models: mathematical formulations and solutions. *J. Atmos. Sci.*, **29**, 11-37.

____, and W. A. Heckley, 1981: Cold and warm fronts in baroclinic waves. *Quart. J. Roy. Meteor. Soc.*, **107**, 79-90.

Kao, R. L., 1987: Baroclinic instability and frontogenesis. M. S. Thesis, Department of Earth and Atmospheric Sciences, Purdue University, W. Laf., IN., 109pp.

Shuman, F. G, 1957: Numerical methods in weather prediction: II, smoothing and filtering. *Mon. Wea. Rev.*, **85**, 357-361.

Stone, P. H., 1966: Frontogenesis by horizontal wind deformation fields. *J. Atmos. Sci.*, **23**, 455-465.

Sun, W. Y., 1980: A forward-backward time integration scheme to treat internal gravity waves., *Mon. Wea. Rev.*, **108**, 402-407.

____, 1984: Numerical analysis for hydrostatic and nonhydrostatic equation of inertial-internal gravity waves. *Mon. Wea. Rev.*, **112**, 259-268.

____, and W. -R, Hsu, 1984: Numerical simulation of atmospheric mesoscale convection, Supercomputer applications, Plenum Publishing Corporation, New York, U.S.A., pp. 145-157.

____, and W. R. Hsu, 1988: Numerical study of cold air outbreak over the warm ocean. *J. Atmos Sci.*, **45.**, 1205-1227.

____, 1989: Modified Eady waves and frontogenesis, Part I: Linear stability analysis. *TAO*, **1**, 363-378.

Williams, G. P., 1974: Generalized Eady waves. *J. Fluid. Mech.*, **62**, 643-655.

Williams, R. T., 1967: Atmospheric frontogenesis: A numerical experiment. *J. Atmos. Sci.*, **24**, 627-641.

____, 1968: A note on quasi-geostrophic frontogenesis. *J. Atmos. Sci.*, **25**, 1157-1159.

____, and J. Plotkin, 1968: Quasi-geostrophic frontogenesis. *J. Atmos. Sci.*, **25**, 201-206.

改造之Eady波與鋒生
第二部分　非線性積分

商文義
美國普渡大學地球和大氣科學系

摘　要

改造之Eady波在定切變及拋物線型之位溫剖面流體中的穩定性分析已在本文之第一部分中討論。在這一部分中我們將使用發展於普渡大學之非線性模式來研究由第一部分中所得之不穩定波演化過程。雖然因拋物線型之位溫剖面使高層大氣有較强之成層使得模擬出長波（在第一部分中以模Ⅰ相稱）擾動的振幅在接近高層時小於靠近底層。但是長波發展成鋒面後，其氣壓與溫度的最大擾動產生於模擬範圍內的最高或最低處；此結果與Williams和Hoskin對一般Eady波所討論的相似。至於短波（在第一部分中以模Ⅱ相稱）它需要較長的時間發展成鋒面，且被限制在低層大氣中發展。由模式所模擬的短波相速正如本文第一部分所預測之情形一樣比一般之斜壓波慢很多。

從穩定性分析及非線性積分皆證實了地面波／鋒面當低層大氣之成層微弱時，在幾天內可發展並達到有限的振幅。本文所得之結果可能與在冬天時發展於黑潮和東中國海之中尺度擾動有關。